Evaluating moisture transfer properties of wood by inverse analysis of moisture content profiles determined during drying by X-ray attenuation

Sahbi Ouertani, Antoine Stéphan, Patrick Perré, Clément L'hostis, Romain Rémond

Evaluating moisture transfer properties of wood by inverse analysis of moisture content profiles determined during drying by X-ray attenuation

Sahbi Ouertani[a], Antoine Stéphan[a], Patrick Perré[b,c], Clément L'Hostis[d], Romain Rémond[a*]

[a]*Université de Lorraine, INRAE, LERMAB, F-88000 Epinal, France*

[b] *Université Paris-Saclay, CentraleSupélec, LGPM, Gif-sur-Yvette, France*

[c] *Université Paris-Saclay, CentraleSupélec, LGPM Centre Européen de Biotechnologie et de Bioéconomie (CEBB), Université Paris-Saclay, F-5110 Pomacle, France*

[d]*FCBA, F-77420 Champs-sur-Marne, France*

* romain.remond@univ-lorraine.fr;

Evaluating moisture transfer properties of wood by inverse analysis of moisture content profiles determined during drying by X-ray attenuation

Abstract

An X-ray density analyzer was used to determine the evolution of the moisture content (MC) profiles of a wood board during drying. Tests were performed on quartersawn boards of five wood species (oak, beech, Scotch pine, birch, alder) of two thicknesses (20 and 40 mm) dried at low temperature. The water vapor diffusion coefficient and liquid permeability of each wood species were determined by inverse analysis of the profiles using a computational model of coupled heat and mass transfer. These parameters were also measured by classical methods for validation purposes. The inverse method gives values close to the measured ones when using the evolution of the moisture profile, but also quite remarkably when using only the evolution of moisture at the core of the board. On the contrary, the method is less accurate when using only the average kinetics as experimental information.

Keywords*:* Heat and mass transfer, diffusivity, permeability, computational model, porous media.

Introduction

When a plank of wood dries, the moisture content first changes near the exchange surfaces, triggering an internal moisture migration. This results in the establishment of a non-uniform moisture content (MC) field decreasing over time, which ultimately tends towards the equilibrium moisture content. These fields are at the origin of a non-uniform shrinkage field, that generates the drying stresses.[1] Cracks can occur when the stress level exceeds the breaking strength of the wood, which causes significant losses in value for manufacturers. The evolution of the MC profiles is therefore a key feature to work on to reduce drying stress.

The shape of the moisture profiles depends on the convective drying conditions experienced on the exchange surfaces and the internal resistance to moisture migration within the porous medium. The latter varies during the drying process, mainly as a function of the

local MC. During low temperature drying, the two main mechanisms involved in water migration are capillary migration and the combined diffusion of bound water and water vapor. At the beginning of drying, as liquid water is removed at the surface, a liquid pressure gradient develops that drives the liquid from the inner part of the material towards the exchange surface in accordance with the generalized Darcy's law, with the capillary pressure as the driving force.[2–4] The efficiency of the capillary pressure gradient depends on the intrinsic permeability (K) and the relative liquid permeability, which can be expressed as a function of the saturation of the wetting phase.[2] In the hygroscopic range, both water vapor and bound water fluxes occur, driven by the moisture concentration gradient (diffusion). Both phenomena, which act together at the pore level, establish a global parameter at the macroscopic scale, the diffusion coefficient that can be defined using the gradient of MC as the driving force. Again, this lumped diffusion coefficient is a function of the moisture content and temperature.

The intrinsic permeability and the water diffusion coefficient therefore appear to be two key transfer properties that determine the shape of the moisture profiles. Conventional techniques for measuring these properties in wood have been presented, for example, in Siau[3] or in Perré[2]. In steady-state methods, the experimental principle is quite simple and usually involves controlling the pressure gap (liquid, gas or water vapor) through the sample and determining the resulting flow rate. In transient methods, the experimental principle consists in imposing a change in relative humidity for diffusivity or in total pressure for permeability to create a transient mass flux through the sample. The transfer properties are then determined either by an analytical solution, which assumes simpler physics and perfect climatic conditions, or by an inverse method by minimizing the difference between observed and computed moisture content. Noted that several studies[5,6] have shown that measuring the water diffusion coefficient under steady state or transient conditions gives similar values in

the T or R direction of wood. Besides, it was shown that the models used to simulate the evolution of moisture content must account for coupled heat and mass transfers for the transfer properties to be accurately determined.[5,7,8] One of the advantages of inverse analysis the possibility to account for the actual climatic conditions, integrating all experimental perturbations to be considered in the identification process.

The inverse analysis has been used successfully in several studies, mainly to determine the water diffusion coefficient and sometimes its dependence on moisture content.[6–14] . However, few studies have matched calculated and experimental moisture content in wood above fiber saturation to determine the liquid transfer properties of wood.[15,16] These previous works may differ by the experimental device used to follow the evolution of moisture content. The experimental data used can be the mass change of the sample during a wetting or drying stage.[7,10,12,14] Perre et al.[11] proposed a variant of this family of methods by measuring the relative humidity on the sealed face of the sample after a sudden variation in the relative humidity on the opposite side. The experiment used by Kouchade[6] is based on measuring the electrical resistance of a wood sample in a transient state which is then compared with those computed by a heat and mass transfer model from the moisture content field in the specimen. The inverse analysis of Liu et al.[9] is based on the moisture profiles measured by Simpson[17] using a destructive method in which a section of northern red oak was removed periodically during drying. This section was then sliced in small pieces along the profile, each of which was weighed twice (flat slicing and after oven-drying) to determine its MC. Eriksson et al.[13] used X-ray CT-scanning to determine the moisture content distribution within a Norway spruce board during drying. CT-scanning has the advantage of being non-destructive and non-invasive method that do not interfere with local moisture transfers.

The aim of this work is to extract the water diffusion coefficient and the intrinsic permeability from the evolution of the moisture profile measured in the board thickness

during drying. The first part of this paper describes the drying tests and the sample preparation. Several species and two thicknesses were selected to obtain contrasted MC profiles and kinetics. The X-ray density analyzer is then introduced, along with the method of determining the moisture profile from the density profile. A last part describes the determination of the moisture transfer properties, which were both measured experimentally by dedicated methods or identified by inverse analysis.

Material and methods

Samples preparation

Five wood species were studied in this paper: oak (*Quercus robur*), beech (*Fagus sylvatica*), Scotch pine (*Pinus sylvestris*), birch (*Betula pendula*), and alder (*Alnus incana*). The samples were taken from freshly cut logs harvested in the Vosges region of France. All trees were 30- to 35-years old. The oak samples came from the heartwood part of the log, whereas the Scotch pine samples were taken from the sapwood part. For the other species—birch, alder, and beech—it was more difficult to give this information since they are species with white heartwood where it is difficult to detect the sapwood by color. Each bar was cut into two pieces, one of which was planned down to a thickness of 40 mm and the other to 20 mm. These sets of samples can be considered as twin samples because they came from the same annual rings. The final sample dimensions were 40 or 20 mm in the tangential direction (T) and 50 mm in both the radial (R) and longitudinal (L) directions (Figure 1). Sample sizes were chosen to accommodate the sample carriage dimensions of the X-ray density analyzer.

Four out of the six faces of the wood samples were covered with a self-adhesive aluminum foil that forced 1-D moisture transfer along the sample thickness, i.e., in the tangential direction. For better adhesion, the aluminum sheets were coated with epoxy resin on the cross-sections. No resin was used on the lateral faces so that the aluminum sheet could be

removed for each X-ray scan.

(Figure 1)

Drying experiments

To perform the drying tests, the samples were placed on a perforated tray in a climatic chamber (Memmert HPP260, Germany) (Figure 2). Three axial fans, positioned vertically at the rear of the climate chamber, stirred the air to homogenize temperature and relative humidity throughout the chamber volume. The samples have their exchange surfaces parallel to the fan flow. This climate chamber was set to 40°C and 65% RH.

The external heat transfer coefficient, which plays a crucial role in defining the external resistance to transfer, must be supplied as input parameter to focus the inverse analysis on internal transfers. The value of this parameter in our experiments was assessed in the same chamber using the sponge method.[18] A value of about 18 W m^{-2} K^{-1} was determined for this parameter.

(Figure 2)

During drying, the samples were periodically removed from the climate chamber and scanned with the X-ray system. The frequency was 1 or 2 scans per day at the beginning and decreased during drying down to ca. 3 scans per week. At each scan, the dimensions and mass were measured using a digital caliper (±0.02 mm) and a digital balance (±0.001 g). To limit the moisture exchange with the environment during manipulation, the sample was wrapped in an aluminum sheet. The total time outside the climatic chamber for one scan did not exceed 10 minutes. The disturbance of the climatic conditions in the chamber at each measurement was limited to only a few minutes by a very fast return to the set conditions.

Determination of the moisture content profile from the density profile

X-ray density analyzer

The laboratory X-ray density analyzer system DAX-5000 (Fagus-GreCon, Germany) was used to determine the density profiles along the thickness. This system was designed for the density analysis of wood composite panels using small samples (50 x 50 mm^2) based on a fast and a non-destructive method. The attenuation of X-rays transmitted through the sample width is related to the raw sample density. During the scanning period, the sample moves perpendicularly to the X-ray beam (Figure 1). The manufacturer's specifications indicate a density accuracy of ±0.5% over a measurement range up to 1500 kg/m^3. The sample was moved in front of the source by steps of 0.02 mm. The scanning rate measurement was automatically adjusted according to the material density and ranged from 0.05 to 1 mm/sec. For each scan, the actual sample dimensions and mass were measured as described above. These data were entered into the user interface of the X-ray system to give the average density of the scanned sample. The density profile was therefore determined relative to the average value obtained from the data entered by the user, ensuring that the mean density of the density profile is consistent with the measured density of the sample. Prior to each scan, the aluminum foil was removed from the LT sides of the sample to avoid spurious attenuation of X-rays (Figure 1). At the end of the drying experiments, the oven-dried sample mass was determined after 24 hours in an oven at 103±2°C.

Calculation of MC profiles from density profiles

Many works successfully applied X-ray techniques to determine moisture content fields in wood.[19–21]. The method consists of measuring the change of X-ray attenuation through the material at two different MC, the first at the unknown MC and the second at a known one (here, the oven-dried state). The change of X-ray intensity (CT number) depends on the

density change of the material, that is used to determine the change in MC. The difficulty to convert the change in attenuation into a change in MC lies in the shrinkage of wood: indeed, the change in attenuation depends on two parameters, the change in MC and the change in local wood density. Different methods have been proposed in the literature to overcome this limitation.[20] In our case, simplifications of the above-mentioned methods stand thanks to 1-D profiles and X-ray beam along the radial direction of wood.

The scanned thickness (T-direction of the sample) is considered along the *x*-axis, and the origin is one exchange surface of the sample. The measured local density at position *x* and time *t* ($\rho(x,t)$) can be expressed as a function of the local anhydrous density ($\rho_0(x)$):

$$\rho(x,t) = \rho_0(x) \cdot \big(1 + X(x,t)\big) \cdot \frac{V_0(x)}{V(x,t)} \qquad (1)$$

with $V_0(x)$ the local anhydrous volume, $V(x,t)$ the local wet volume at time *t*, and $X(x,t)$ the local moisture at time *t*.

In our case, this equation can be simplified by assuming that the local anhydrous density is constant and equal to the global anhydrous density of the sample measured at the end of the test (i.e., $\rho_0(x) = \rho_0$). This is a realistic assumption since we have a quartersawn sample, the X-ray beam thus passes through similar annual rings, whatever the *x*-coordinate. As we did not have markers to follow the local displacement along the T-direction, we could not know the change in local volume at each *x*-coordinate during drying. However, in the absence of a moisture gradient in the R- and L-directions (one-dimensional moisture transfer), the dimensional change in the T-direction is considered as free shrinkage. This is not strictly true due to the Poisson effect induced by the radial shrinkage. However, radial shrinkage is roughly half that of tangential shrinkage and, in addition, the small width of our samples

limits the intensity of the Poisson strain. The local swelling at the *x*-coordinate could then be estimated as follows:

$$\varepsilon_T(x,t) = G_T \cdot \frac{X_b(x,t)}{X_{FSP}} \qquad (2)$$

with X_{FSP} the fiber saturation point (about 30%), $X_b(x,t)$ the bound water content which is the minimum value between X_{FSP} and the local moisture content $X(x,t)$ and G_T the swelling coefficient in the tangential direction around the *x*-coordinate. This coefficient was assumed to be equal to the global shrinkage coefficient measured on the sample between the saturated and oven-dried states.

Moreover, the dimensional change in the R-direction is restrained shrinkage. Thus, the width crossed by the X-ray beam was assumed to be independent of the *x*-coordinate and equal to the global width of the sample measured at each scan (i.e., $l_R(x,t) = l_R(t)$).

Finally, in the L-direction, the shrinkage is negligible and the dimension l_L is independent of MC (i.e., $l_L(x,t) = l_L(x) = l_L^0(x)$).

Under these assumptions, the following relationship was obtained:

$$\rho_X(x,t) = \rho_0 \cdot \frac{\big(1 + X(x,t)\big)}{\big(1 + \varepsilon_T(x,t)\big)} \cdot \frac{l_R^0}{l_R(t)} \qquad (3)$$

where l_R^0 is the global width of the sample in the R-direction measured at the oven-dried state.

The measured density profiles were converted to MC profiles using Equation (3).
Noted that the measurement of a one-dimensional MC profile, as proposed here, provides much poorer information than the previously mentioned works using X-ray computed

tomography. However, its measurement speed (a few tens of seconds per sample), moderate cost and simplicity offer an interesting alternative to complex, costly equipment

Direct measurements of intrinsic permeability and water diffusion coefficient

Experimental measurements

The air permeability and water vapor diffusivity were measured on the same samples. They were cut with a hole-saw from the 40 mm thick dried boards used in the previous part to obtain between three and five 19 mm diameter samples per species. The axis of the cylinder was along the tangential direction of the wood, and the sample thickness (l^T) along this direction was 9 mm.

The air permeability was measured using the specific device ALU-CHA developed by Agoua[22] and used in numerous previous works.[23–25] The method consists of applying a constant air pressure gap on both sides of the sample and measuring the resulting air flow. The air permeability was then calculated for each sample using Darcy's law (Eq.4).

$$K = \frac{Q \cdot \mu \cdot \ell \cdot P}{S \cdot \Delta P \cdot \bar{P}} \qquad (4)$$

where K is the intrinsic permeability (m^2), Q the volumetric flux (m^3/s), μ the dynamic viscosity of the air ($1.97.10^{-5}$ Pa. s), ℓ the sample thickness (m), P the pressure at which the flux Q is measured (Pa), S the transverse section of the sample (m^2), $\Delta P = P_2 - P_1$ the pressure gap between faces 1 and 2 of the sample, and $\bar{P} = (P_1+P_2)/2$ the average pressure inside the sample (Pa).

The water vapor diffusivity was determined at steady state using the cup method at 35°C. The method consists of applying a constant relative humidity gap on both sides of the sample (75% internal cup–40% external cup) and measuring the resulting mass flow. The RH

at the bottom of the sample was maintained with a saturated saline solution of NaCl, and RH at the top was controlled by a climatic chamber. Each wood sample was assembled with the airtight PVC-CHA device attached to the glass of the test tube.[23,24,26] The assembly was weighed periodically, about once every two days. The mass flow through the sample was estimated from the linear zone of the curves of the mass loss. The dimensionless diffusivity f is simply estimated using Fick's law with water vapor density as the driving force (Eq. 5):

$$f = \frac{Q \cdot l^T \cdot R \cdot T}{D_V \cdot S \cdot \Delta RH \cdot P_{VS}(T) \cdot M_V} \qquad (5)$$

where Q is the measured mass flow (kg.s^{-1}), S the transverse section of the sample (m²), M_v the molar mass of vapor (0.018 kg.mol^{-1}), ΔRH the variation of RH at the top and bottom surfaces of the sample (-), T the sample temperature (308 K), R the ideal gas constant (8.314 J.mol^{-1}.K^{-1}), l^T the thickness of the sample (m), D_v the water vapor diffusivity in air (here 2.81E-5 m². s^{-1}), and P_{vs} the saturated vapor pressure (Pa).

Correction factors were applied to the measured water vapor diffusivity to account for the resistance vapor diffusion of the air layer between the sample and the salt solution and the "masked edge". They have been extensively described in several works.[23,26,27]

In many works, the water flux is expressed with regard to the gradient of moisture content as the driving force and the bound water diffusivity D_b (m²/s). For isothermal configurations, the value of D_b can be related to that of f (the gradient of water vapor density as the driving force) by using the slope of the water sorption isotherm curve:

$$D_b = \frac{f \cdot D_V \cdot M_V}{\rho_0 \cdot R \cdot T} \cdot \frac{\Delta P_V}{\Delta X} \qquad (6)$$

where ΔX and ΔP_V are, respectively, the gaps of the moisture content (expressed as a decimal (kg/kg)) and of the partial vapor pressure (Pa) consistent with the sorption isotherm

in the range of the test. In the conditions of this work, ΔX, estimated from the sorption isotherm of Almeida et al.[28], equals 6.6% and ΔP_V equals 1930 Pa.

However, this coefficient is known to increase with the MC and the effect should be taken into account with regards to the large range of MC values undergone during drying. The thermo-hygro activation of diffusion was studied by Stamm[29] and is expressed by an exponential function:[3,30]

$$D_b = C \cdot \exp\left(9.8 \cdot X_b - \frac{4300}{T}\right) \qquad (7)$$

where C is a constant specific to the wood species; X_b is the bound water fraction (kg/kg) and T the temperature (K).

The diffusion coefficient was determined in this work at 35°C and with an equilibrium moisture content (EMC) estimated from the sorption isotherm of Almeida et al.[28] at 13.2% and 6.6% for the bottom and top faces, i.e., an average MC of 9.9%. The *C* value of Eq.(7) was estimated under these conditions for each species in this work from the measured dimensionless diffusivity *f* (Eq.5), which was converted to D_b (Eq.6). A ratio D_0 was introduced to compare the value of C specific to the studied species with that used by Perré and Turner[30] to model softwood drying.

$$D_0 = C/\exp(-9.9) \qquad (8)$$

Determination by an inverse analysis

The shape of the theoretical MC profiles strongly depends on the permeability and diffusion coefficient. This dependence was used to determine these parameters by minimizing the gap between the experimental and predicted MC profiles. The fast one-dimensional version of *TransPore*[30], a comprehensive computational model for heat and mass transfer in porous

media, was used. It has been successfully used in previous works to identify the diffusion coefficient of wood and wood-based panels during unsteady regimes.[11] The actual conditions seen in the samples are implemented as boundary conditions to simulate the drying of the samples. The code uses as input parameters the measured density, the initial moisture content, sample thickness and other parameters and functions given in Perré and Turner[30]. Noted that the same expressions were used for all species for the relative permeability and capillary functions. The *TransPore* code uses here the capillary pressure function proposed by Spolek and Plumb[31] for softwoods and the relative permeability functions proposed for wood by Perré and Turner[30]. This is a strong assumption, but very few expressions have been proposed in the literature and their experimental determination remains a very challenging task.[2,6] This means that the identified intrinsic permeability is likely to depend on the choice of these functions. Consequently, only the resulting liquid migration coefficient (permeability times relative liquid permeability times derivative of the capillary function) is relevant to express liquid migration.

As the version of *TransPore* used here does not account for shrinkage, the input thickness is that of the sample at the end of drying. For the comparison measurement-simulation, the experimental profiles were all reduced to the thickness used in the *TransPore* code by assuming a constant homotheticity ratio for each scan. The measured MC values (here, more than 1500 points per scan along the thickness) were linearly interpolated on the mesh nodes (here typically 51 control volumes).

The objective function δ quantifies the MSE (Mean Squared Error) between the experimental and simulated values. A weighted average of the error on the kinetics and the error on MC profile was used:

$$\delta = A \cdot \zeta_1 + B \cdot \zeta_2 \qquad (9)$$

with

$$\zeta_1 = \sum_{i=1}^{n} \left(\overline{MC}_i^{calc} - \overline{MC}_i^{meas} \right)^2 \qquad (10)$$

$$\zeta_2 = \sum_{i=1}^{n} \left(\sum_{j=1}^{m} \left(Gap_j^{calc} - Gap_j^{meas} \right) \right)^2 \qquad (11)$$

ζ_1 is the error on the mean kinetics while ζ_2 is the error in the shape of the MC profiles. A and B quantify the proportion of ζ_1 and ζ_2 in the objective function by respecting the equality $A+B=1$. $\overline{MC}_i^{calc}$ and $\overline{MC}_i^{meas}$ are respectively the predicted and measured average MC. Gap_j^{calc} and Gap_j^{meas} are respectively the measured and predicted gaps between the average MC value $\overline{MC}_i$ and the MC at each scanning position MC_j (Figure 3). Indices *i* and *j* are the discrete time and the discrete position in the board thickness, respectively, which correspond to the available experimental values. *n* is the total number of measurements, and *m* is the total number of positions scanned by the experimental X-ray device.

(Figure 3)

In this work, another objective function has been studied, a variant of the previous one, which is simply defined from the difference of the local MC at a given position *j* between the measurement and the simulation:

$$\delta = \sum_{i=1}^{n} \left(MC_{i,j}^{calc} - MC_{i,j}^{meas} \right)^2 \qquad (12)$$

The unknown parameters, such as the liquid permeability and the diffusion coefficient in this work, are modified by the downhill-Simplex method[32] that iterates to minimize the objective function.

Results and discussion

An example of MC profiles calculated from X-ray density profiles

As an example, Figure 4 depicts the conversion of X-ray density profiles to MC profiles using Eq. (3) for the 20 mm thick oak sample. Noted that preliminary tests were carried out to qualify the efficiency of the X-ray device to detect the density variation within the samples due to the change in MC. One of these tests is shown in Appendix 1.

At the beginning of drying, the density profile is flat at about 1,150 $kg \cdot m^{-3}$, which corresponds to an initial MC of about 80%. Then, as drying progresses, the peripheral samples zone dries first, which turns into parabolic profiles of density (Figure 4a). The sample thickness decreases during drying (Figure 4) due to shrinkage that begins when the peripherical zone of the section enters the hygroscopic range (about 30% MC). The shrinkage progresses by reaching deeper layers from the exchange surfaces and stabilizes as the MC tends toward the equilibrium MC. Consistently, the density tends towards a flat profile at about 795 $kg \cdot m^{-3}$ at the end of drying, which corresponds to an equilibrium MC of about 12%. The shape of these profiles obviously depends on the transfer properties of the material, the permeability for liquid water migration, and the diffusivity for bound water migration.

(Figure 4)

Direct measurements of permeability and diffusivity

To better understand the drying behavior of the investigated wood species and to validate the inverse procedure, these two parameters, permeability and diffusivity, were measured on the three to five samples prepared for each section. The air permeability was plotted as a function of the dimensionless diffusivity factor *f* for all samples (Figure 5). This figure confirms the well-known variability of wood, both among and within species. However, clear trends can be observed between species. Oak samples, in the heartwood part, present the lowest values of

both vapor diffusivity and permeability, confirming the difficulty of water migration both above and below the FSP. At the opposite end, Scotch pine has large values for both parameters, which anticipates a very easy drying. The three other species (alder, birch, and beech) are along the line between these two extreme behaviors. For beech, the values of *f* and K are quite scattered, but one can observe that, compared to the two other species, the permeability is significantly lower at similar diffusivity. This would indicate a less efficient liquid migration. This scattering could also be partly explained by the sample cross-section (Appendix 2), in which the annual rings are not perfectly orthogonal to the left exchange surface.

The results clearly show that the diffusion coefficient decreases with the increasing wood density. Scotch pine wood with a density of 407 $kg \cdot m^{-3}$ presents the highest dimensionless diffusivity factor *f* of about 0.005, while oak with a density of 727 $kg \cdot m^{-3}$ presents the lowest *f*-value of about 0.002. The measured values are given in Appendix 3.

(Figure 5)

Drying kinetics and moisture field within the board

Impact of wood species

Figure 6 shows very contrasting drying kinetics for 20 mm thick samples. The initial MC values of Scotch pine sapwood samples are very high at about 200%. This value is close to the maximum MC that can be estimated from the sample porosity by assuming it was fully saturated in water.[19] Its anhydrous density is quite low, about 420 $kg \cdot m^{-3}$, with a very large annual ring (Appendix 2). Despite its very high MC, Scotch pine sapwood dries very quickly due to its high permeability and dimensionless diffusivity *f* (Figure 6). It is the first to reach the equilibrium moisture content (EMC) around 12% (Figure 6). The moisture profiles of Figure 7a support these analyses. Scotch pine presents almost flat moisture profiles

throughout drying, i.e., very little moisture gradient between the core and the periphery of the sample, reflecting a very low resistance to internal transfer for both free and bound water.

Among the hardwoods, the alder sample enters the second drying phase after 7 hours of drying and the beech sample after 1 day. This corresponds to a MC at the periphery below the FSP (around 30%), together with the beginning of shrinkage, which reduces the sample thickness (Figures 7b, c). The longer first drying phase for beech seems to indicate a lower resistance to liquid migration than alder, which was not confirmed by the permeability measurement (Figure 5). Note that, in the present study, the intrinsic permeability was measured on a dry sample using gas as the fluid phase, but lower values can be obtained with liquid, as observed for beech by Perré and Karimi[33]. This difference depends on the species.[2] This could also be explained by the assumption of the same relative permeability and capillary functions for all species.

Birch, on the other hand, has slightly slower kinetics as it starts at a lower initial MC. Indeed, its properties (Figure 5 and Appendix 3) revealed a lower air permeability and diffusivity than alder, Scotch pine, and some beech samples. Its initial MC is lower, and it seems to enter the second drying phase early (before 10 hours), with a decreasing drying rate. The core of the sample remains at a high MC for a longer time, and the periphery quickly enters the hygroscopic domain, below the FSP (Figure 7d). The intensity of moisture transfer at the exchange surfaces seems too high compared to the resistance to internal moisture transfers. The sample thickness starts to reduce after 7 hours of drying, and continues to decrease at each acquisition.

As expected, oak wood has the slowest drying kinetics (Figure 6). It also enters the second drying phase very early (before 10 hours) (Figures 8a,c). For oak, we find the trends observed in birch but with an even greater contrast, with flat moisture profiles in the central part and steeper at the periphery. This is the characteristic shape of a drying front that

propagates from the exchange surface towards the center. After 6 days of drying, the central part is still above the FSP.

(Figure 6)

(Figure 7)

Impact of sample thickness

Figures 8a,b depict the evolution of MC at 1 mm from the exchange surface and at different depths defined for fixed proportions of the thickness (i.e., one-fifth, one-third and one-half of the thickness). The figure shows that the drying kinetics is strongly impacted by the thickness of the sample. For example, the drying time of the 40 mm thick oak sample to reach 20% of the average MC is 2.5 times longer than that of the 20 mm thick sample, and the thick board has a much higher MC gradient. Figures 8c,d show that, after 22 hours of drying, only the first 5 mm at the periphery of the board has started to dry and it shows a high moisture gradient, while for the central part of the board, the moisture profile is flat and remains close to the initial MC. The water contained in the central part of the thick board still maintains a high MC at 10 mm from the exchange surface after 70–77 hours of drying, while it decreases for the thin board.

This increased internal resistance to water migration of thick boards causes the MC profiles to be steeper, which should result in higher stress levels via the shrinkage. In industrial drying, it is well known that thick boards are more prone to mechanical degradation.[1]

(Figure 8)

Determination of permeability and diffusivity by an inverse method

By minimizing the objective function, the liquid permeability and the diffusion coefficient were determined by the computational model. The results of the drying of 40mm thick

samples were used for this identification. Different configurations have been studied in this work.

- Case 1: The optimization is done both on the average kinetics and on the shape of the moisture profiles with the same weighting factor in the objective function Eq. (9) (i.e., A = B = 0.5),
- Case 2: The optimization is done only on the average kinetics, i.e., A = 1 and B = 0,
- Case 3: The optimization is done only on the kinetics of the MC at the core of the board (Eq. (12), with j = index value at mid-thickness).

Figure 9 depicts the comparison of the measured and calculated moisture profiles after optimization of the objective function (case 1). Note that, for clarity, just a subset of MC profiles has been plotted. The code captures well the contrasting moisture profile shapes and kinetics during the drying of these different species. Once the surface attains the hygroscopic range, a bell-shaped profile develops with two zones developing inside the board, marked by an inflexion point on the MC profiles. In the inner zone, the liquid migration prevails and in the surface zone, the diffusion of water vapor and bound water takes place. For some species, the inflection point appears to be at a higher MC on the measured profiles than on the simulated ones. It is always around the saturation point of the fibers (FSP) for the model, with a value around 30%, which corresponds to the MC where the product of the relative liquid permeability times the derivative of capillary function tends towards zero, while this inflection point appears a little higher for alder, oak, and beech.
(Figure 9)

Figure 10 compares the measured values with those identified by the inverse method for the different species and for the configurations 1 to 3 specified above. The large dispersion

of the measured gaseous permeability values leads the standard deviation (error bar in Figure 10) to exceed the mean value for all species except for alder. Figure 10a shows that the identification of the permeability gives values very close to the measured values for these five species for cases 1 and 3. Regarding the optimization, according to cases 1 and 3, it allows one to correctly capture the D_0 values of these different species, except for Scotch Pine. For this last species, the flat profiles of the MC and the insufficient number of measurements at the end of drying (Figure 10) give too little weight to D_0 in the minimization of the objective function. The identification of the diffusion coefficient D_0 seems to be less accurate in case 2 (Figure 10b). The use of the mean MC kinetics alone does not seem restrictive enough to find the pair of values D_0 and K.

The quality of the measurements of these two values obtained by the inverse method with only one measurement of MC at the core of the board (case 3) is remarkable. This method had already been used successfully in the past to measure the diffusion coefficient based on the RH measured at the back face of the sample.[11] Based on the kinetics of the core MC during drying, this method also seems to be relevant for estimating both the diffusion coefficient and the permeability.

(Figure 10)

Conclusion

In this work, a protocol was proposed to use an X-ray density analyzer to assess the evolution of the moisture content profiles of boards during drying. These profiles were used to identify by inverse analysis the permeability and the moisture diffusivity. These identified values were compared with the values obtained from direct measurements. The following conclusions were drawn:

- the X-ray density analyzer is a convenient tool to determine MC profiles during drying, and is an interesting alternative to more sophisticated tools such as X-ray computed tomography,
- the five species studied cover a large range of behavior and physical parameter values,
- thanks to a comprehensive heat and mass transfer code, two moisture transfer parameters can be identified from the experimental MC profiles, and the values obtained agree with those obtained by direct measurement, except for the diffusion coefficient of Scotch Pine due to insufficient measurements at the end of drying,
- more remarkably, using the time evolution of the core MC value only is enough to identify these two parameters.

Acknowledgments

ADEME is a partner in the project and is co-funding, with FCBA, a grant for a thesis on the use of intermittent energy for wood drying by using an intelligent control system.

References

(1) Rémond, R.; Passard, J.; Perré, P. The Effect of Temperature and Moisture Content on the Mechanical Behaviour of Wood: A Comprehensive Model Applied to Drying and Bending. *Eur. J. Mech. - ASolids* **2007**, *26* (3), 558–572. https://doi.org/10.1016/j.euromechsol.2006.09.008.

(2) Perré, P. *Fundamentals of Wood Drying*, ARBOLOR.; Nancy, France, 2007.

(3) Siau, J. F. *Transport Processes in Wood*; Springer Series in Wood Science; Springer-Verlag: Berlin Heidelberg, 1984. https://doi.org/10.1007/978-3-642-69213-0.

(4) Perré, P.; Rémond, R.; Almeida, G.; Augusto, P.; Turner, I. State-of-the-Art in the Mechanistic Modeling of the Drying of Solids: A Review of 40 Years of Progress and Perspectives. *Dry. Technol.* **2023**, *41* (6), 817–842. https://doi.org/10.1080/07373937.2022.2159974.

(5) Agoua, E.; Zohoun, S.; Perré, P. A Double Climatic Chamber Used to Measure the Diffusion Coefficient of Water in Wood in Unsteady-State Conditions: Determination

of the Best Fitting Method by Numerical Simulation. *Int. J. Heat Mass Transf.* **2001**, *44* (19), 3731–3744. https://doi.org/10.1016/S0017-9310(01)00022-9.

(6) Kouchade, A. C. Mass diffusity of wood determined by inverse method from electrical resistance measurement in unsteady state. Ph.D Diss, ENGREF, Nancy, France, 2004. https://pastel.hal.science/pastel-00000888.

(7) Jannot, Y.; Bal, H. M.; Degiovanni, A.; Moyne, C. Influence of Heat Transfer on the Estimation of Water Vapor Diffusion Coefficient in Transient Regime. *Int. J. Heat Mass Transf.* **2021**, *177*, 121558. https://doi.org/10.1016/j.ijheatmasstransfer.2021.121558.

(8) Perré, P.; Challansonnex, A.; Colin, J. On the Importance of Heat and Mass Transfer Coupling for the Characterization of Hygroscopic Insulation Materials. *Int. J. Heat Mass Transf.* **2019**, *133*, 968–975. https://doi.org/10.1016/j.ijheatmasstransfer.2018.12.105.

(9) Liu, J. Y.; Simpson, W. T.; Verrill, S. P. An Inverse Moisture Diffusion Algorithm for the Determination of Diffusion Coefficient. *Dry. Technol.* **2001**, *19* (8), 1555–1568. https://doi.org/10.1081/DRT-100107259.

(10) Olek, W.; Perré, P.; Weres, J. Inverse Analysis of the Transient Bound Water Diffusion in Wood. *Holzforschung* **2005**, *59* (1), 38–45. https://doi.org/10.1515/HF.2005.007.

(11) Perré, P.; Pierre, F.; Casalinho, J.; Ayouz, M. Determination of the Mass Diffusion Coefficient Based on the Relative Humidity Measured at the Back Face of the Sample During Unsteady Regimes. *Dry. Technol.* **2015**, *33* (9), 1068–1075. https://doi.org/10.1080/07373937.2014.982253.

(12) Kouchade, A. C.; Passard, J.; Perre, P. Inverse Method Using TransPore 1-D Code for The Mass-Diffusivity Determination In Wood. JMSSE. **2018**, 6(4), 845-850.

(13) Eriksson, J.; Johansson, H.; Danvind, J. Numerical Determination of Diffusion Coefficients in Wood Using Data from CT-Scanning. *Wood Fiber Sci.* **2006**.

(14) Olek, W.; Rémond, R.; Weres, J.; Perré, P. Non-Fickian Moisture Diffusion in Thermally Modified Beech Wood Analyzed by the Inverse Method. *Int. J. Therm. Sci.* **2016**, *109*, 291–298. https://doi.org/10.1016/j.ijthermalsci.2016.06.023.

(15) Couture, F.; Jomaa, W.; Puiggali, J.-R. Relative Permeability Relations: A Key Factor for a Drying Model. *Transp. Porous Media* **1996**, *23* (3), 303–335. https://doi.org/10.1007/BF00167101.

(16) Rémond, R.; Baettig, R.; Perré, P. Identification of Relative Permeability Curves for Softwood Using a Computational Model and Moisture Content Profiles Determined by X-Ray Absorptiometry; Budapest, Hungary, 2006; vol vol. C : 1793-1797.

(17) Simpson, W. T. Determination and Use of Moisture Diffusion Coefficient to Characterize Drying of Northern Red Oak (Quercus Rubra). *Wood Sci. Technol.* **1993**, *27* (6), 409–420. https://doi.org/10.1007/BF00193863.

(18) Challansonnex, A.; Casalinho, J.; Perré, P. Non-Fickian Diffusion in Biosourced Materials: Experimental Determination of the Memory Function Using Minute Samples. *Constr. Build. Mater.* **2019**, *224*, 560–571. https://doi.org/10.1016/j.conbuildmat.2019.07.013.

(19) Martin, B.; Colin, J.; Lu, P.; Mounkaila, M.; Casalinho, J.; Perré, P.; Rémond, R. Monitoring Imbibition Dynamics at Tissue Level in Norway Spruce Using X-Ray Imaging. *Holzforschung* **2021**, *75* (12), 1081–1096. https://doi.org/10.1515/hf-2020-0269.

(20) Couceiro, J. X-Ray Computed Tomography to Study Moisture Distribution in Wood. Ph.D Diss, Luleå tekniska universitet, Sweden, 2019.

(21) Lindgren, O.; Nilsson, L.O. X-Ray and Gamma-Ray. In *Methods of measuring moisture in building materials and structures : State-of-the-art report of the RILEM Technical Committee 248-mmb*; Springer, 2018; Vol. 26, pp 157–169.

(22) Agoua, E. Diffusivité et Perméabilité Du Bois: Validation de Méthodologies Expérimentales et Prise en Compte de Paramètres Morphologiques Simples pour la Modélisation Physique. *PhD Diss ENGREF Nancy Fr.* **2001**.

(23) Ouertani, S.; Simo-Tagne, M.; Rémond, R. Sorption Isotherms and Moisture Transfer Properties of Seven Central Africa Hardwood Species. *Wood Mater. Sci. Eng.* **2023**, *18* (2), 507–516. https://doi.org/10.1080/17480272.2022.2051736.

(24) Tarmian, A.; Remond, R.; Dashti, H.; Perré, P. Moisture Diffusion Coefficient of Reaction Woods: Compression Wood of Picea Abies L. and Tension Wood of Fagus Sylvatica L. *Wood Sci. Technol.* **2012**, *46* (1), 405–417. https://doi.org/10.1007/s00226-011-0413-3.

(25) Agoua, E.; Perré, P. Mass Transfer in Wood: Identification of Structural Parameters from Diffusivity and Permeability Measurements. *J. Por. Media* **2010**, *13* (11), 1017-1024. DOI:10.1615/JPorMedia.v13.i11.80

(26) Zohoun, S.; Agoua, E.; Degan, G.; Perre, P. An Experimental Correction Proposed for an Accurate Determination of Mass Diffusivity of Wood in Steady Regime. *Heat Mass Transf.* **2003**, *39* (2), 147–155. https://doi.org/10.1007/s00231-002-0324-9.

(27) Claesson, J.; Hagentoft, C.-E.; Wadsö, L. Masked Edge Effects When Measuring Diffusion Coefficients with the Cup Method. *Polym. Eng. Sci.* **1994**, *34* (10), 821–826. https://doi.org/10.1002/pen.760341007.

(28) Almeida, G.; Remond, R.; Perre, P. Hygroscopic Behaviour of Lignocellulosic Materials: Dataset at Oscillating Relative Humidity Variations. *J. Build. Eng.* **2018**, *19*, 320–333.

(29) Stamm, A. J. Bound-Water Diffusion into Wood in the Fiber Direction. *For. Prod J* **1959**, *9*, 27–32.

(30) Perré, P.; Turner, I. W. A 3-D Version of TransPore: A Comprehensive Heat and Mass Transfer Computational Model for Simulating the Drying of Porous Media. *Int. J. Heat Mass Transf.* **1999**, *42* (24), 4501–4521.

(31) Spolek, G. A.; Plumb, O. A. Capillary Pressure in Softwoods. *Wood Sci. Technol.* **1981**, *15* (3), 189–199. https://doi.org/10.1007/BF00353471.

(32) Nelder, J. A.; Mead, R. A Simplex Method for Function Minimization. *Comput. J.* **1965**, *7* (4), 308–313. https://doi.org/10.1093/comjnl/7.4.308.

(33) Perré, P.; Karimi, A. Fluid Migration in Two Species of Beech (Fagus Silvatica and Fagus Orientalis): A Percolation Model Able to Account for Macroscopic Measurements and Anatomical Observations. *Maderas. Ciencia y tecnología* **2002**, *4* (1), 50–68.

Appendix 1. Qualification of the MC determination

Figure 11 presents the scanned density profile of two twin triangular beech samples whose respective MC varies. One is in the anhydrous state, and the other is close to full saturation (110% of MC). The dashed lines represent the density estimated from the global density of each sample, the mass-to-volume ratio, and their dry-to-wet proportion according to the *x*-coordinate.

The comparison between the scanned density and the theoretical density is excellent which demonstrates the ability of the X-ray device to measure density variations of wood due to a change of MC.

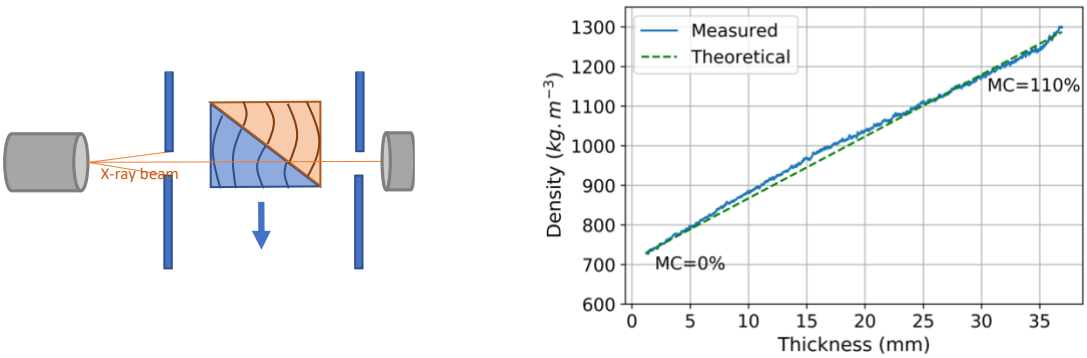

Figure 11. Comparison of the theoretical and X-ray scanned density profile of twin triangular beech samples placed side by side each with different moisture content.

Appendix 2. Example of the cross-section image of investigated samples

Scotch pine Birch Beech Alder Oak

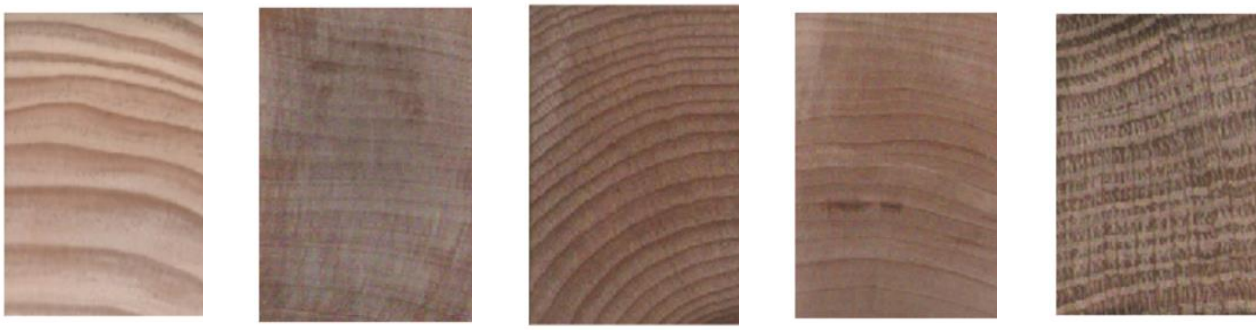

Appendix 3.

Values of permeability and dimensionless diffusivity factor *f* (Eq.5), bound water diffusion coefficient D_b (Eq.6), and factor D_0 (Eq.8) for the different species in this work. The identified value of D_0 indentified by the inverse method (case 1) is also given in the last column of each property.

	N°	ρ_0 (kg/m3)	Gaseous permeability (m²)						Diffusivity					
			Value per sample	Average value per species	SD	Inverse method Case n°			*f* (-) Eq.5	D_b ($m^2.s^{-1}$) Eq.6	D_0 (-) Eq. 8	D_0 (-) Inverse method Case n°		
						1	2	3				1	2	3
Scotch pine	1	407	3.4E-16	3.2E-15	5 E-15	6.6E-15	1.4E-14	6.3E-15	0.00479	6.9E-11	0.97	3.95	2.1	2.31
	2	407	9.0E-15						0.00628	9.0E-11	1.28			
	3	407	3.4E-16						0.00454	6.5E-11	0.92			
Birch	1	634	3.5E-16	1.4E-16	1.4E-16	1.0E-16	1.5E-16	2.0E-16	0.00455	4.2E-11	0.59	0.79	1.12	0.85
	2	628	4.2E-17						0.00310	2.9E-11	0.41			
	3	628	1.2E-16						0.00270	2.5E-11	0.36			
	4	628	3.8E-17						0.00300	2.8E-11	0.39			
Alder	1	469	5.3E-16	5.2E-16	2 E-16	6.4E-16	4.2E-16	5.1E-16	0.00386	4.8E-11	0.68	0.95	1.25	0.85
	2	470	7.5E-16						0.00377	4.7E-11	0.66			
	3	470	2.6E-16						0.00353	4.4E-11	0.62			
	4	470	5.4E-16						0.00408	5.1E-11	0.72			
Beech	1	665.9	8.6E-17	1.0E-16	1.5E-16	1.4E-16	1.2E-16	9.4E-17	0.00534	4.7E-11	0.66	0.37	0.47	0.37
	2	663.6	8.9E-18						0.00425	3.7E-11	0.53			
	3	663.6	3.6E-16						0.00504	4.4E-11	0.63			
	4	663.6	3.3E-18						0.00328	2.9E-11	0.41			
	5	671.8	3.6E-17						0.00342	3.0E-11	0.42			
Oak	1	744.9	2.9E-18	6.4E-18	9.7E-18	3.0E-17	1.5E-16	2.6E-17	0.00222	1.7E-11	0.25	0.34	1.12	0.35
	2	693.9	2.1E-17						0.00166	1.4E-11	0.20			
	3	768.0	1.1E-18						0.00226	1.7E-11	0.24			
	4	734.3	6.0E-19						-	-	-			

List of tables

(-)

List of figures

Figure 10. Comparison of permeability and diffusion coefficient D_0 (Eq. 8) along the tangential direction measured experimentally or identified by the inverse method with different objective functions (cases 1–3). The error bar represents the standard deviation of the measurements. For Scotch pine, the identified D_0 values are between 2.1 and 3.9.

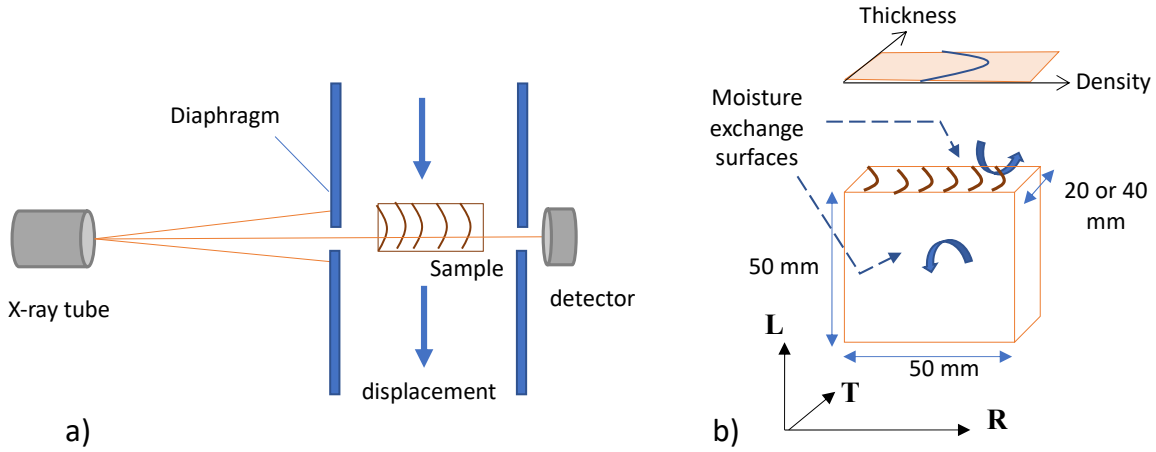

Figure 1. Schematic view of the sample scanning in the X-ray density analyzer (a), wood sample with only two moisture exchange surfaces, the lateral face being coated with an epoxy resin and aluminum foil tape (faces in the LT and RT planes) (b).

Figure 2. The climate chamber used for the drying tests in with the exchange surfaces of the samples exposed along the fan flow.

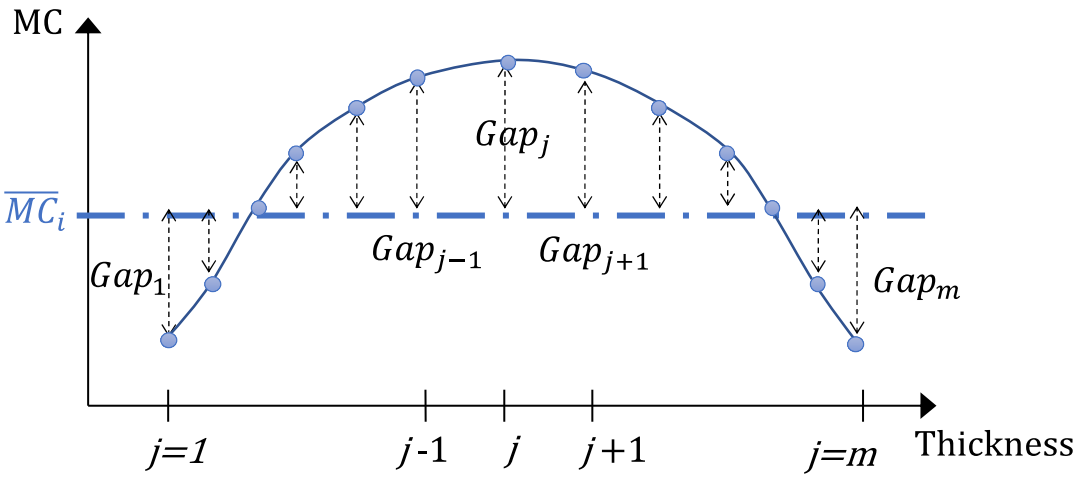

Figure 3. Gaps and average MC for a given MC profile in the board thickness at time *i*. Gap j is the difference between the local MC at the scan position *j* and the average $\overline{MC}$.

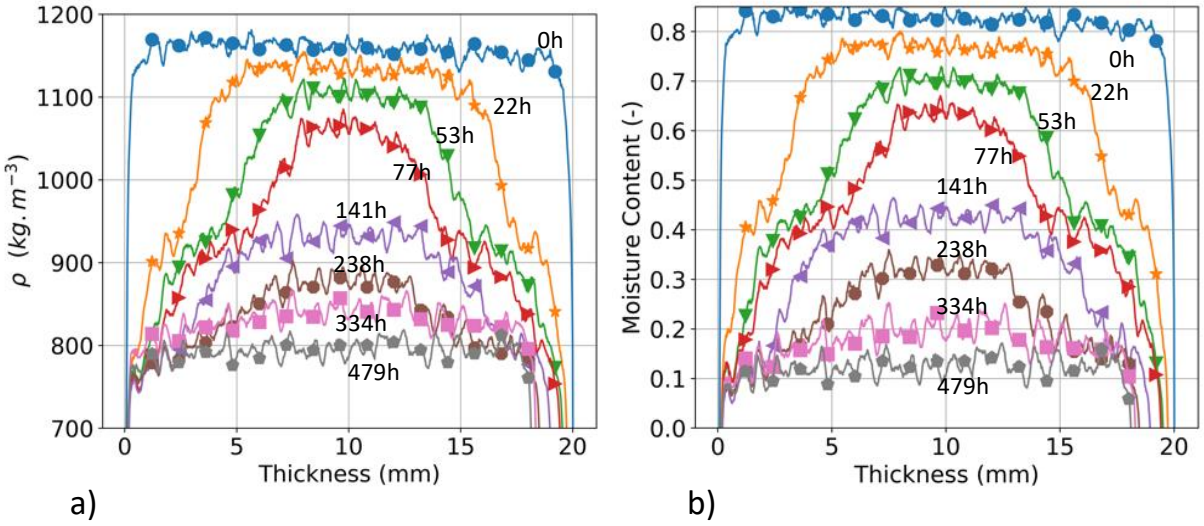

Figure 4. Example of the transformation of a) density profiles measured by X ray scanning to b) MC profiles of oak wood during drying.

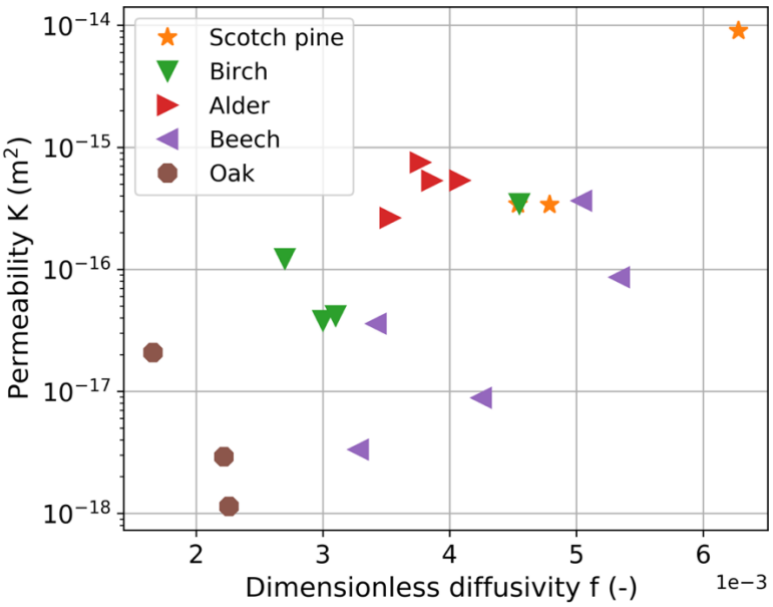

Figure 5. Relationship between gas permeability and dimensionless diffusivity factor in the tangential direction of the studied woods.

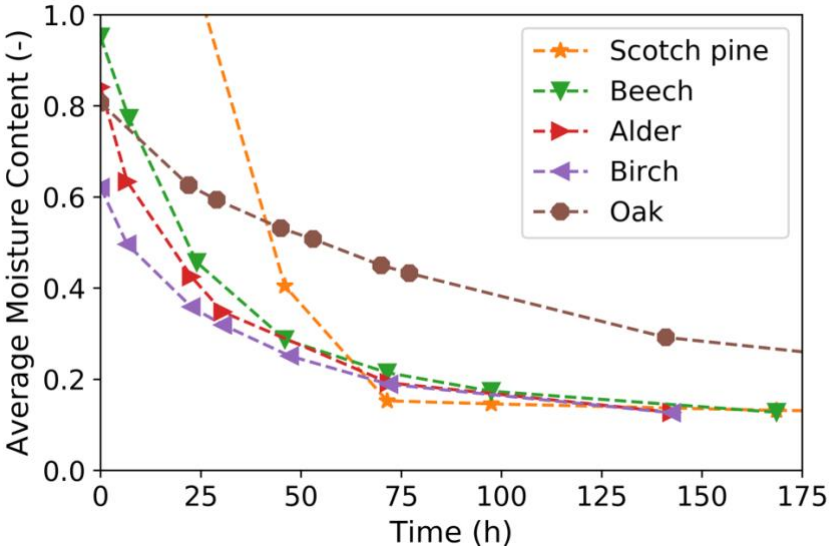

Figure 6. Drying kinetics of the five wood species studied, 20 mm thick samples.

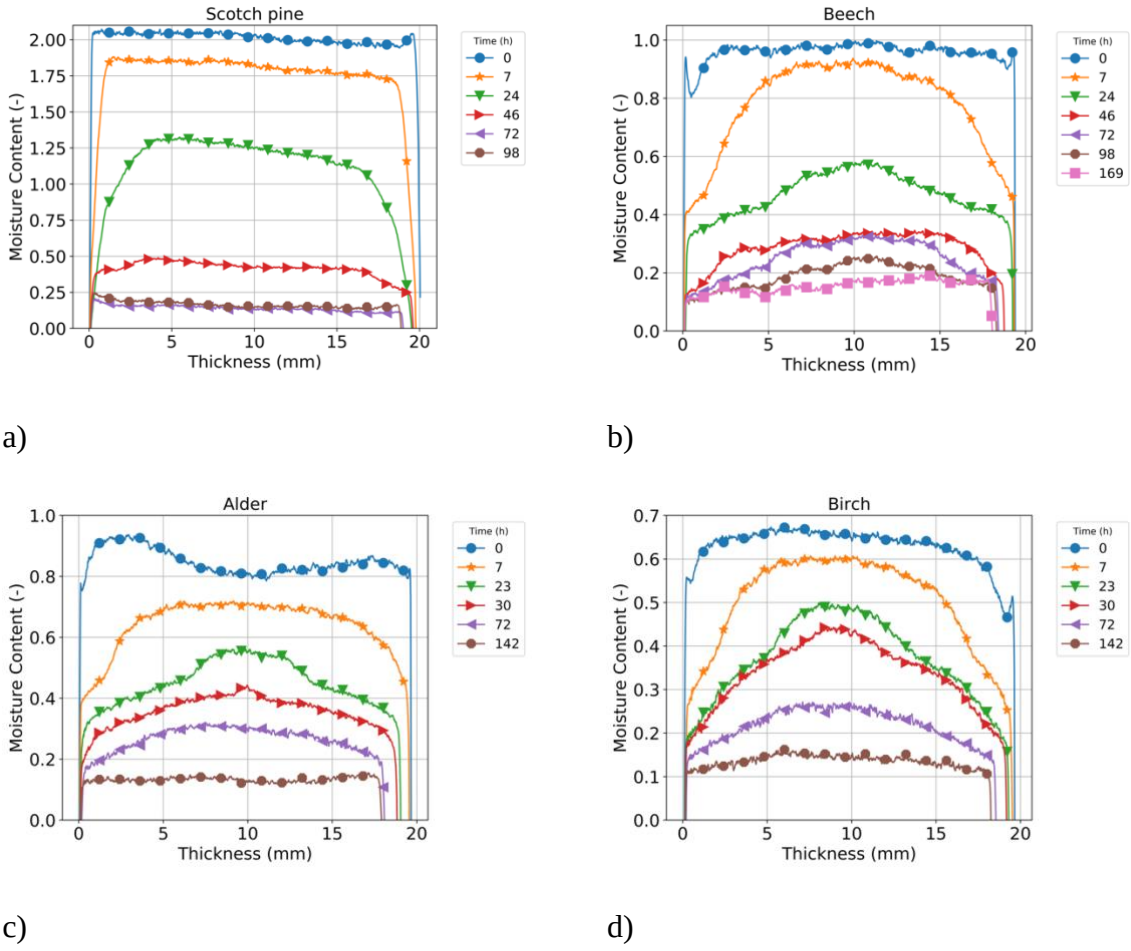

Figure 7. Evolution of the moisture content profile along the sample thickness of 20 mm, for a) Scotch pine, b) beech, c) alder, d) birch.

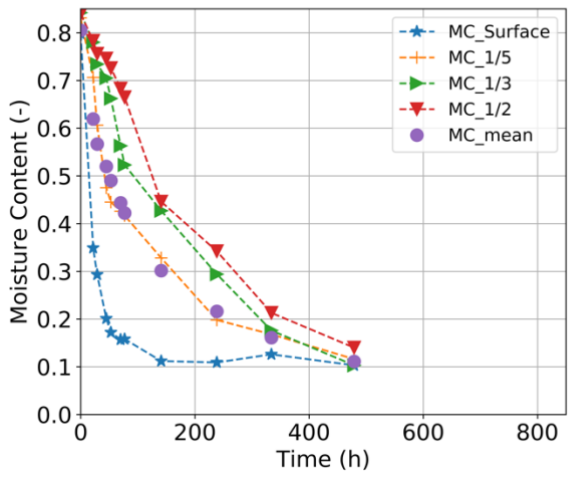

a)

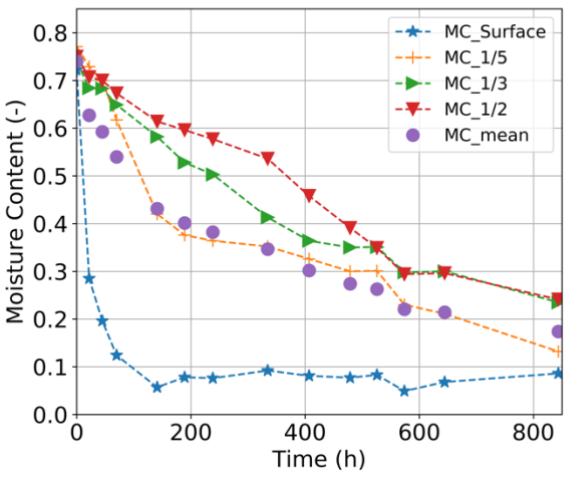

b)

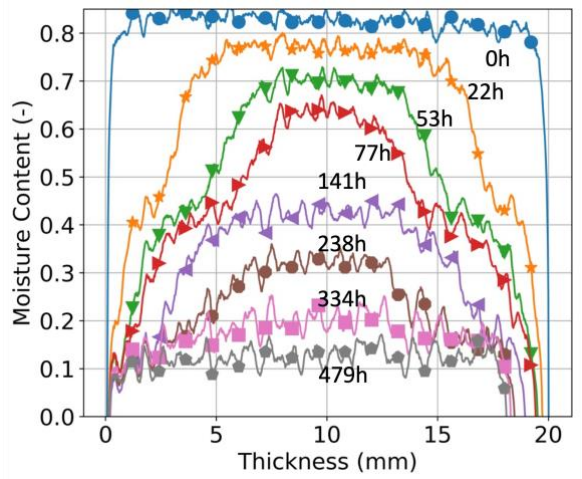

c)

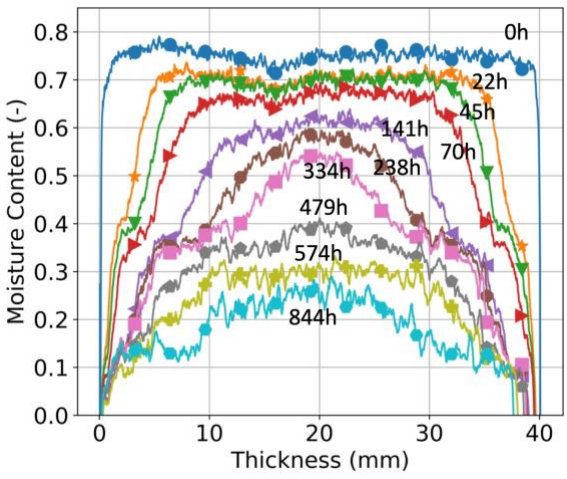

d)

Figure 8. Comparison of drying kinetics and MC profiles of thin (a, c) and thick oak boards (b, d).

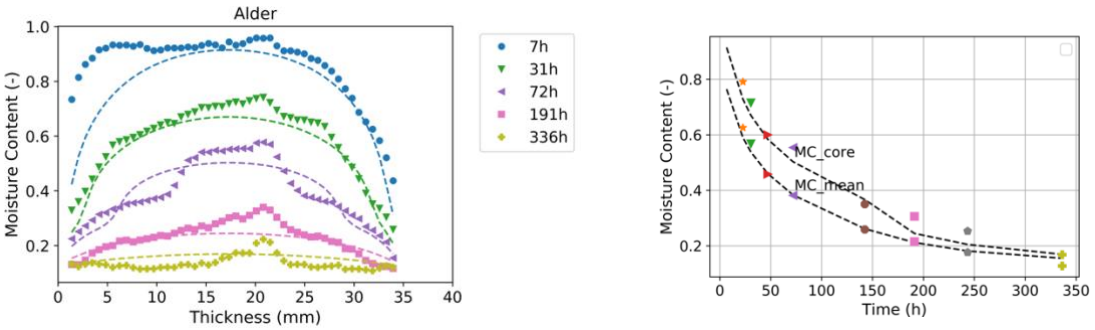
Alder
Moisture Content (-)
Thickness (mm)
7h
31h
72h
191h
336h
MC_core
MC_mean
Time (h)

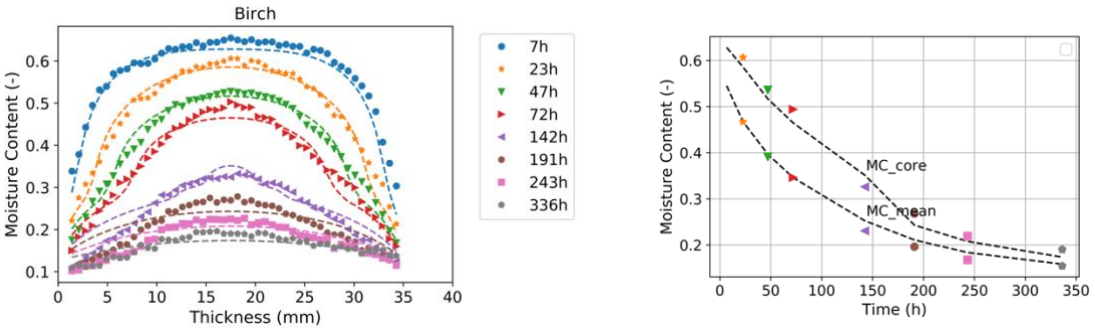
Birch
Moisture Content (-)
Thickness (mm)
7h
23h
47h
72h
142h
191h
243h
336h
MC_core
MC_mean
Time (h)

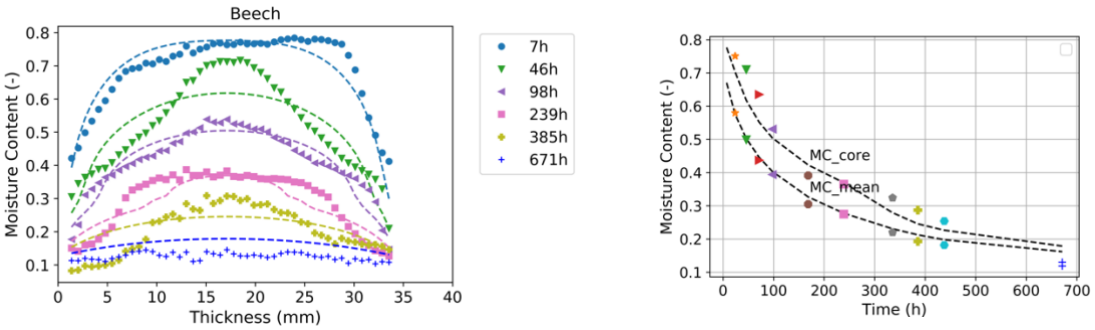
Beech
Moisture Content (-)
Thickness (mm)
7h
46h
98h
239h
385h
671h
MC_core
MC_mean
Time (h)

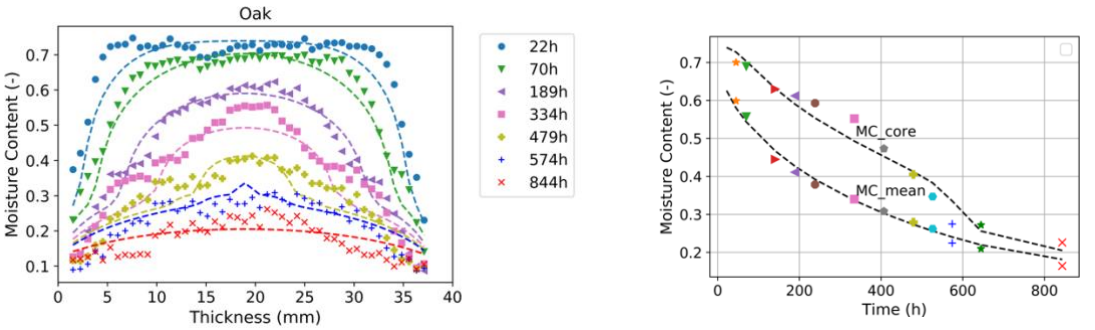
Oak
Moisture Content (-)
Thickness (mm)
22h
70h
189h
334h
479h
574h
844h
MC_core
MC_mean
Time (h)

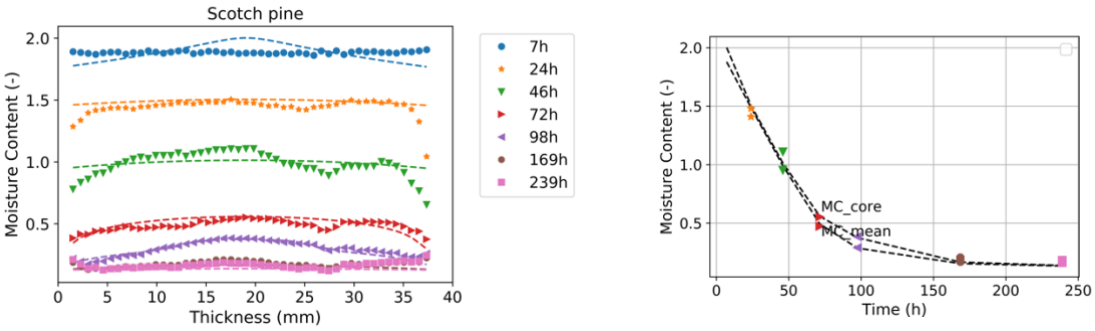

Figure 9. Simulated (dashed lines) and measured (markers) moisture profiles (left) for 40mm thick samples. The corresponding kinetics of MC at the core and average MC are shown on the right.

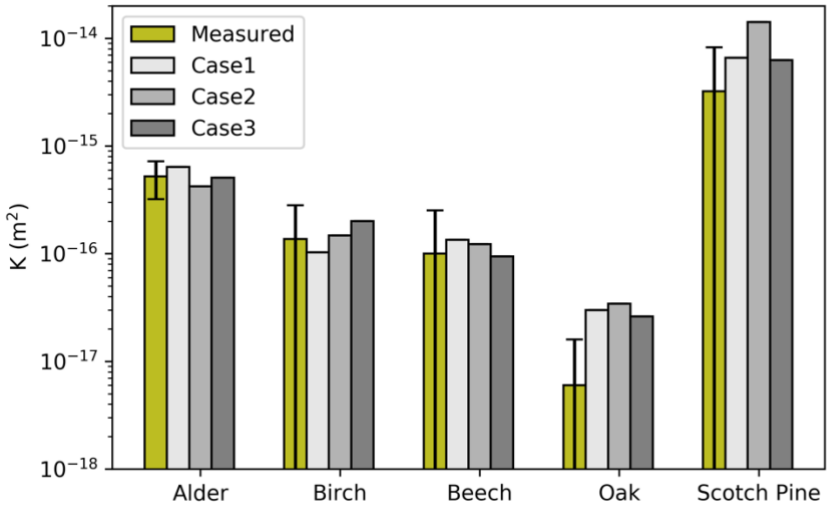

a)

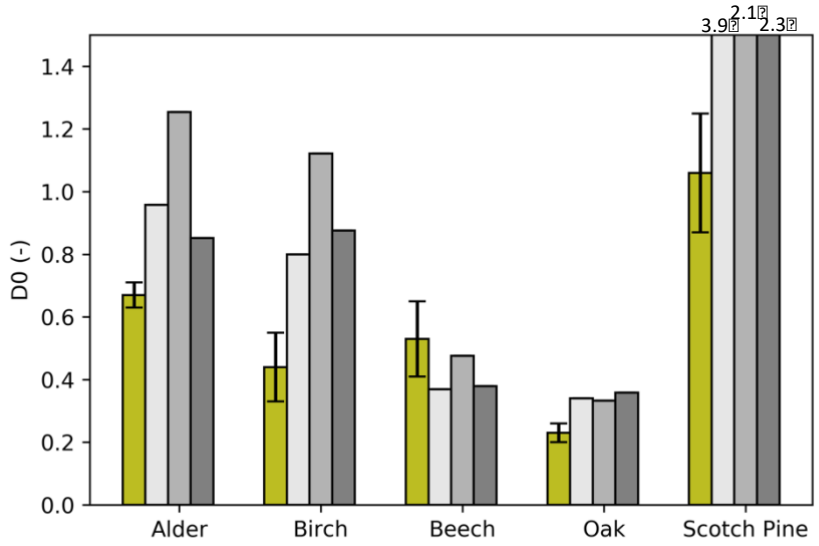

b)

Figure 10. Comparison of permeability and diffusion coefficient D_0 (Eq. 8) along the tangential direction measured experimentally or identified by the inverse method with different objective functions (cases 1–3). The error bar represents the standard deviation of the measurements.